

Local Cracking-Induced Scalable Flexible Silicon Nanogaps for Dynamically Tunable Surface Enhanced Raman Scattering Substrates

Chunyan Qu, Qinglei Guo,* Gaoshan Huang, and Yongfeng Mei*

Surface enhanced Raman scattering (SERS), as a promising and convenient analytical tool for molecule sensing, has turned out to be one of the most important applications of plasmonic nanostructures. However, its large-area production, controllability, and adjustability remain significant challenges because of the weak control over the fabrication and spatial arrangement. Herein, a silicon nanogap array-based flexible plasmonic substrate is developed, with capabilities of large-area production, controllable arrangement, and width of nanogaps, by utilizing the standard microfabrication platform, and the fabricated flexible plasmonic substrate is further explored for dynamically tunable SERS for molecular sensing. After experimentally and theoretically optimizing the geometric designs of precursors, a 90×90 silicon nanogap array (over $1 \text{ cm} \times 1 \text{ cm}$) with a yield of about 99.74% is achieved. SERS is realized by depositing Au films onto the silicon nanogap. Dynamically tunable SERS is demonstrated by the thermally induced local stretch or contraction of silicon nanogaps, where the key parameters including Raman enhancement and sensitivity of the molecular sensor can be conveniently adjusted. These presented results significantly expand the scope of engineering opinions for flexible plasmonic nanostructures, which have many envisioned applications especially for environmental monitoring and biochemical detection.

1. Introduction

As a cornerstone of plasmonic nanostructures,^[1] nanogap in between two facing tips or atomic clusters has undergone huge development during the past few decades. Due to the surface plasmon resonance (SPR) induced by the incident light at a certain wavelength, nanogap with a subwavelength width can serve as a “hot spot” thus enhancing the local electromagnetic (EM) field.^[2] Applications of these functional nanogaps mainly manifest in various demonstration examples in several fields, such as molecular sensors,^[3,4] Raman imaging,^[5–7] electrooptic plasmonic modulators,^[8] nanogap electrodes,^[9–11] and other related. Among all these applications, surface enhanced Raman scattering (SERS) has emerged as an advanced and promising analytical tool especially for molecule sensing.^[12] The EM field enhancement, which is considered as the main contributor to SERS, turns out to depend strongly on the geometry and dimension of nanogaps.^[13,14] For instance, nanogaps in between two nanoparticle aggregates contain a large number of hot spots,^[15] which is useful for SERS sensing regardless of the incident polarization. For nanogaps between metallic electrodes, the strongest local field occurs at the situation that the incident EM field is polarized across the nanogap.^[16] Furthermore, a reduction in the width of nanogap leads to an increased local field.^[17] Therefore, the control of geometry and dimension of nanogaps is crucial for their practical applications.

Over the recent years, the rapid development of nanofabrication technology enables the creation of nanogaps either by advanced lithography and etching techniques,^[18–21] or by particularly designed depositions.^[22–25] Although these methods offer good controllability over the resolution and geometry of nanogaps, each method has its own disadvantages, including costly instruments, slow speed, and complex manufacturing designs. One of the most versatile choices relies on controllable cracking for fabricating nanogaps.^[26–28] For example, Pan et al. reported a stress-induced cracking approach to produce scalable suspended Ag/SiN_x nanogaps, as the basis of an SERS substrate for molecular sensing.^[29] With optimized geometrical designs for the initial nanobridge, the width of resulted nanogaps is controllable in a range from sub-10 nm to tens of

C. Y. Qu, Prof. G. S. Huang, Prof. Y. F. Mei
Department of Materials Science
Fudan University
Shanghai 200433, P. R. China
E-mail: yfm@fudan.edu.cn

Prof. Q. L. Guo
School of Microelectronics
Shandong University
Jinan 250100, P. R. China
E-mail: qlguo@sdu.edu.cn

Prof. Q. L. Guo
State Key Laboratory of Functional Materials for Informatics
Shanghai Institute of Microsystem and Information Technology
Chinese Academy of Sciences
Shanghai 200050, P. R. China

Prof. Q. L. Guo, Prof. Y. F. Mei
State Key Laboratory of ASIC and Systems
Fudan University
Shanghai 200433, P. R. China

 The ORCID identification number(s) for the author(s) of this article can be found under <https://doi.org/10.1002/admi.202100661>.

DOI: 10.1002/admi.202100661

nanometers. However, most of the demonstrated SERS substrate is rigid and brittle, which is unavailable for tuning the gap distance, thus inducing weak optical tunability and low sensitivity for the identification of large biomolecules.^[30]

Although numerous theoretical and experimental investigations on mechanisms,^[31,32] fabrications,^[29,33–37] or applications of nanogap-based SERS substrates,^[5,38–40] have been conducted, the simultaneous realization of scalable manufacture and dynamically tunable responses from a flexible nanogap-based SERS substrate remains a significant challenge, which hinders their development in both fundamental nanoscience and practical applications. In this work, on the basis of previous researches,^[30,41] we developed a local-cracking method to fabricate a flexible silicon nanogap array, with scalable production and controllable dimensions, as an additional option in the dynamically tunable SERS substrate for molecular sensing. Optimization of the geometrical designs for silicon ribbons will facilitate the local cracking with the highest yield of about 99.74%. By controlling the loading stress and the temperature, we achieved a 90 × 90 nanogap array with tunable gap width, which was further developed into a flexible SERS substrate. The tunable nanogap width enables the dimensional match between the nanogap width and the molecule diameter, which plays vital roles in acquiring appropriate substrate for the identification of molecules. Dynamically tunable SERS substrate is realized by the thermally induced local stretch or contraction of silicon nanogaps. Appropriate heating treatment of our demonstrated SERS substrate can ensure the complete entrance of biomacromolecules into nanogaps, and the following cooling treatment shrinks the nanogaps to achieve an enhanced Raman signal. This work offers a feasible and effective approach for the identification of molecules with a wide size range, which could benefit environmental monitoring and biochemical detection.

2. Results and Discussions

Flexible silicon nanogaps are fabricated by a local cracking method, as schematically shown in **Figure 1a**. In the beginning, a cleaned silicon-on-insulator (SOI) wafer is patterned into silicon ribbons with periodical “head-to-head” notch pairs via photolithography and reactive ion etching. After the removal of buried silicon dioxide in aqueous hydrogen fluoride (HF), a cured polydimethylsiloxane (PDMS) slab is used to pick-up the released silicon ribbon, which is enabled by the van der Waals force between PDMS and silicon.^[42,43] Notably, the PDMS slab is flexible and elastic, and will deform into a curvy structure during the picking-up process, thus leading to the formation of local cracks in between notch pairs of silicon ribbon because of the concentrated stress at their tips.^[44,45] **Figure 1b** displays a typical flexible silicon nanogap array on PDMS substrate, and the inset shows the scanning electron microscopy (SEM) image of a typical silicon nanogap. Since

the pre-patterned silicon ribbon is defined through photolithography, the obtained flexible silicon nanogap array is scalable to a large area, with the potential for wafer-scale production. To obtain the flexible SERS substrate for molecular sensing, an ultra-thin Au layer is deposited on the silicon nanogap array through electron beam evaporation. As schematically displayed in **Figure 1c**, the Raman scattering peaks of the target object are significantly enhanced from Au/Si nanogaps compared with their counterparts of Au/Si ribbons due to the electromagnetic field enhancement caused by surface plasmon resonance. Notably, the thickness of Au layer can affect the local electromagnetic field of SERS substrate.^[29,46,47] Herein, the thickness of Au layer is set as 30 nm to ensure good SERS properties. Moreover, because of the flexible nature of our fabricated SERS substrate, the width of nanogap can be tuned by stress or temperature, which in turn influences the intensities of Raman peaks.^[1,48] As demonstrated in **Figure 1d**, the intensity of the featured Raman peaks obtained from Rhodamine B (RhB) on flexible SERS substrate increases as the decrease of temperature because of the reduction in nanogap width caused by the PDMS contraction during cooling. Although the increase of temperature will induce a decreased Raman peaks, the obtained Raman signal is still much larger than that of pure Au/Si ribbon (see **Figure S1**, Supporting Information). The demonstrated ability of modulating the nanogap width by our flexible SERS, always with enhanced Raman scattering signals, offers potentials for the identification of molecules with a wide size range.

Although the scale production of pre-patterned silicon ribbon can be conveniently realized via traditional photolithography, the yield of silicon nanogap, defined as the ratio between the number of cracked notch pairs and the number of initial notch pairs, is crucial for their practical applications. To investigate the geometry-dependent yield of silicon nanogaps, we vary key dimensional parameters of the pre-pattern for silicon ribbons, including the distance (labeled as “*a*”) of two notch pairs, and the notch angle (labeled as “*θ*”), as shown in the inset of **Figure 2a**. The width of silicon ribbons (labeled as “*d*”) is set as constant, that is, 50 μm. After picked-up by PDMS, the yields of silicon nanogaps are counted from 20 × 20 notch pairs. As shown in **Figure 2a**, decreases in both *a* and *θ* will result in an increased yield of silicon nanogap, which reaches 99.74% when *a* is 5 μm and *θ* is 30°.

To theoretically explain the relationship between the geometry of silicon ribbons and the yield of silicon nanogap, the yield value is assumed, for simplicity, to be positively related to the stress concentrated at a notch tip. According to the fracture theory,^[44,49] the generalized stress intensity factor of V-shaped notches, K_I^V , as a key parameter that has a positive correlation with the yield of nanogap, is a function of the notch angle *θ*. Therefore, we focus on the relationship between *θ* and K_I^V .

According to the general formulation, pick-up induced stresses in the neighborhood of a V-shaped notch tip for mode I (tension) can be described by three components,^[50]

$$\begin{Bmatrix} \sigma_\omega \\ \sigma_r \\ \tau_{r\omega} \end{Bmatrix} = \lambda r^{\lambda-1} a_l \left\{ \left[\begin{Bmatrix} (1+\lambda)\cos(1-\lambda)\omega \\ (3-\lambda)\cos(1-\lambda)\omega \\ (1-\lambda)\sin(1-\lambda)\omega \end{Bmatrix} + \chi(1-\lambda) \begin{Bmatrix} \cos(1+\lambda)\omega \\ -\cos(1+\lambda)\omega \\ \sin(1+\lambda)\omega \end{Bmatrix} \right] + \left(\frac{r}{r_0}\right)^{\mu-\lambda} \left[(3-\lambda) - \chi(1-\lambda) \right] \begin{Bmatrix} \cos(1+\mu)\omega \\ -\cos(1+\mu)\omega \\ \sin(1+\mu)\omega \end{Bmatrix} \right\} \quad (1)$$

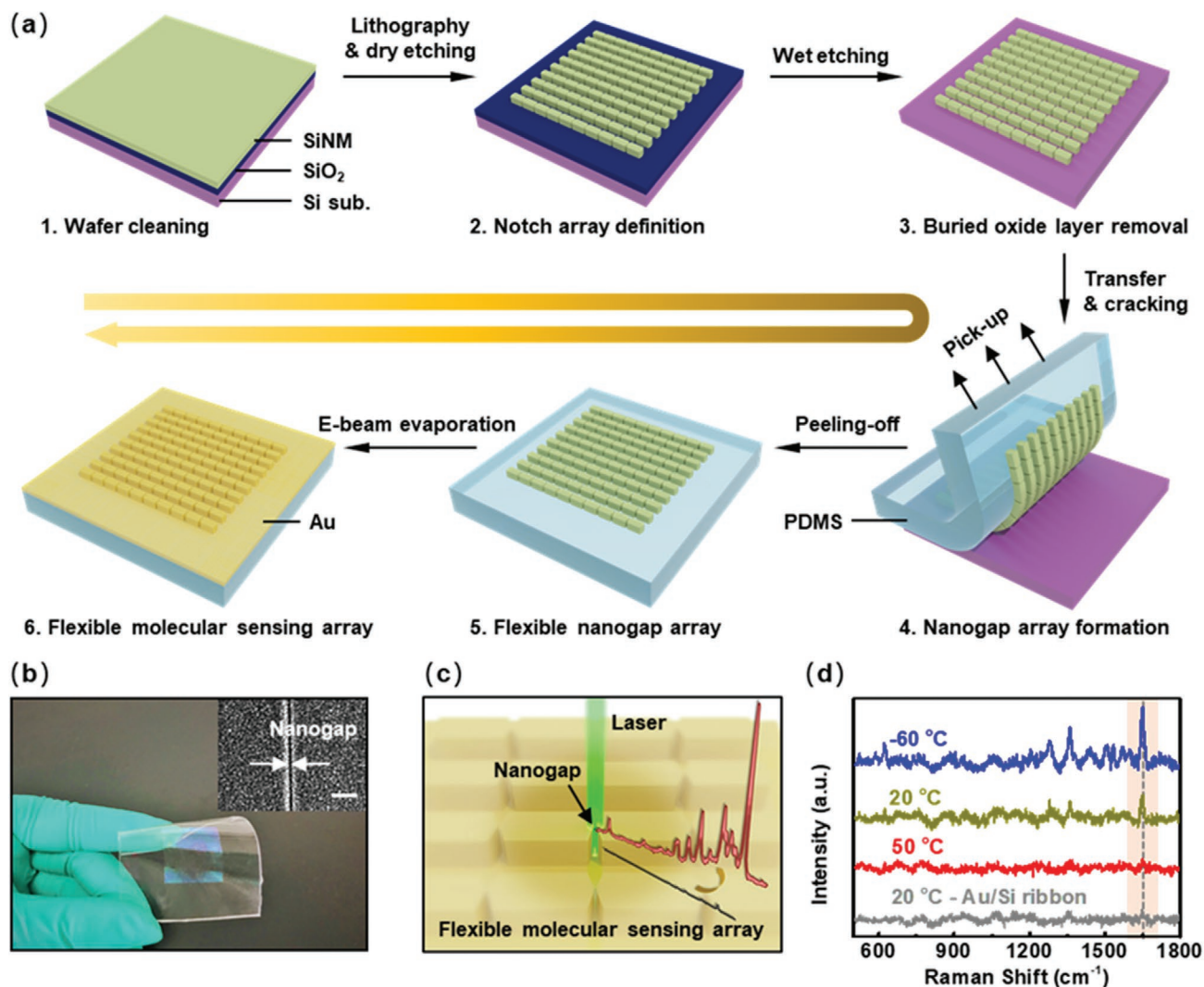


Figure 1. a) Schematic illustration of the fabrication process for a flexible SERS substrate. b) Optical photograph of a flexible 200×200 nanogap array. The inset shows the SEM image of a typical silicon nanogap (scale bar: 200 nm). c) Schematic illustration of a flexible SERS-based molecular sensing array. d) Raman spectra obtained from 10^{-4} M RhB on flexible silicon nanogap-based SERS substrate at low temperature (-60 °C, blue curve), room temperature (20 °C, dark yellow curve), high temperature (50 °C, red curve). The Raman spectrum of 10^{-4} M RhB on an Au/Si ribbon is measured at room temperature (20 °C, gray curve) for comparison.

where σ_ω , σ_r , $\tau_{r\omega}$ are circumferential (tangential) stress, radial stress, and shear stress, respectively, by using the polar coordinates (r, ω) , a_1 is the real part of a complex constant, λ and μ are real coefficients with $\lambda > \mu$ by hypothesis, r_0 is the distance between the notch tip and the origin of the polar coordinate system (for blunt notches, $r_0 \neq 0$), and χ is a coefficient which can be expressed as,

$$\chi = -\frac{\sin(1-\lambda)q\pi/2}{\sin(1+\lambda)q\pi/2} \quad (2)$$

where q is defined as $q = \frac{2\pi-\theta}{\pi}$, $\lambda \in [\frac{1}{2}, 1]$ is the singularity power, which can be solved from the following equation,^[44,49,50]

$$\sin(2\lambda\pi - \lambda\theta) + \lambda \sin(2\pi - \theta) = 0 \quad (3)$$

The variations of λ and χ with θ are extracted through a method similar to the polynomial expansion, as shown in Figure S2, Supporting Information, which is consistent with the previous report.^[44]

For the distribution of stresses in a sharp notch tip (so that the notch radius is set to zero), Equation (1) can be simplified as,^[50]

$$\begin{cases} \sigma_\omega \\ \sigma_r \\ \tau_{r\omega} \end{cases} = \lambda r^{\lambda-1} a_1 \left[\begin{aligned} & \left\{ \begin{aligned} (1+\lambda)\cos(1-\lambda)\omega \\ (3-\lambda)\cos(1-\lambda)\omega \\ (1-\lambda)\sin(1-\lambda)\omega \end{aligned} \right\} + \chi(1-\lambda) \left\{ \begin{aligned} \cos(1+\lambda)\omega \\ -\cos(1+\lambda)\omega \\ \sin(1+\lambda)\omega \end{aligned} \right\} \end{aligned} \right] \quad (4)$$

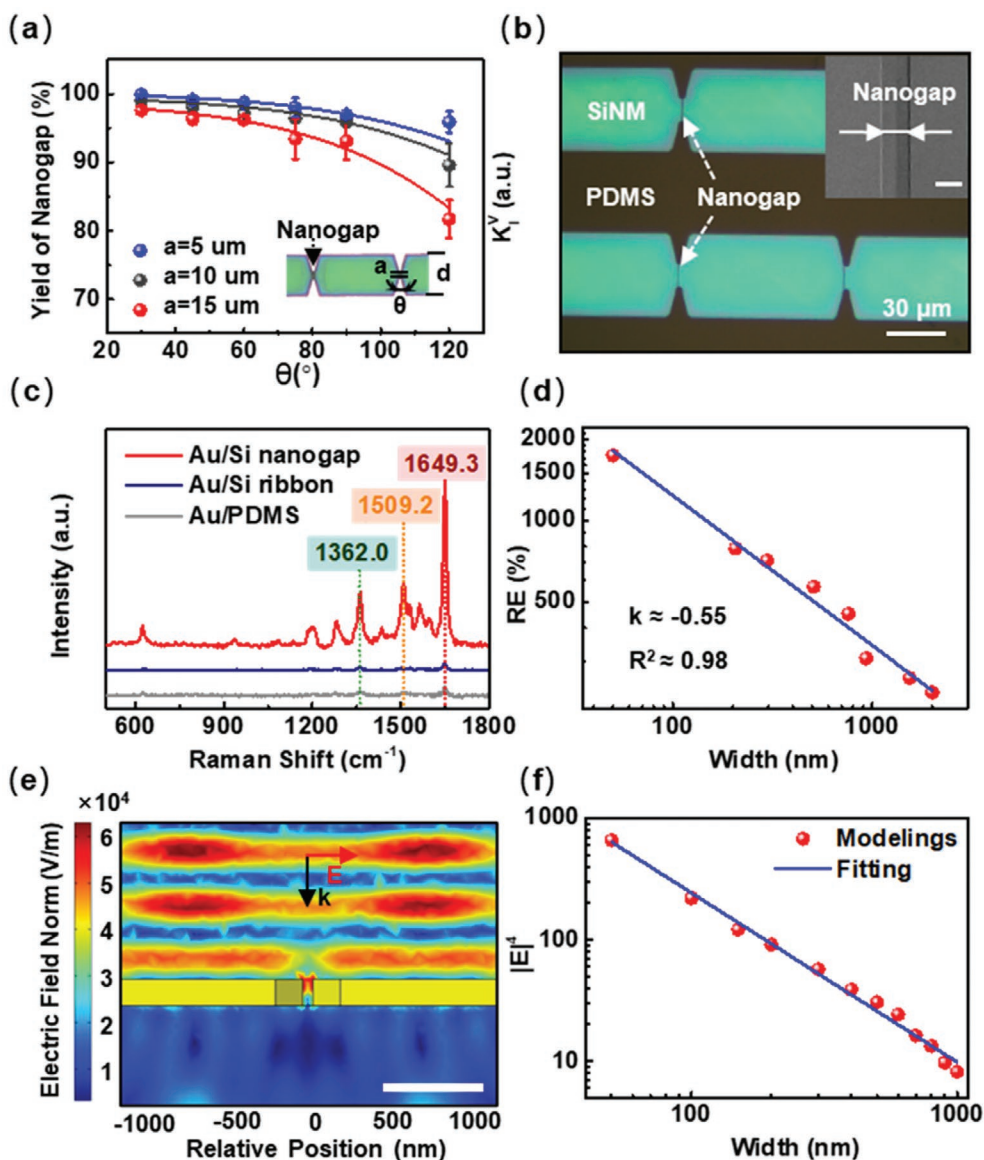


Figure 2. a) Experimental results (dots) and theoretical calculations (solid lines) about the influences of geometrical parameters of the pre-patterned silicon ribbon on the yield of nanogap; $n = 3$ independent experiments. b) Optical microscopy image of silicon nanogaps on the PDMS substrate. The inset shows the SEM image of a typical silicon nanogap (scale bar: 1 μm). c) Raman spectra of 10^{-4} M RhB obtained from Au/Si nanogap (red curve), Au/Si ribbon (blue curve), and Au/PDMS substrate (grey curve). d) Experimental results of the relationship between Raman enhancement (RE) at the Raman shift of 1650 cm^{-1} and the nanogap width. e) Simulation of surface electromagnetic field distribution of Au/Si nanogap (scale bar: 500 nm). The black and red arrows represent the propagation direction (k vector) and the polarization (E field vector), respectively. The width of nanogap is 50 nm. f) Simulated results of the relationship between $|E|^4$ and nanogap width.

Considering that σ_ω is the principal component which is much larger than σ_r and $\tau_{r\omega}$, the circumferential stress σ_ω is focused on in this work. The definition of K_I^V is given by Gross as,^[51]

$$K_I^V = \sqrt{2\pi} \lim_{r \rightarrow 0} (\sigma_\omega)_{\omega=0} r^{1-\lambda} \quad (5)$$

According to Equation (4), $\lim_{r \rightarrow 0} (\sigma_\omega)_{\omega=0}$ can be calculated as,

$$\lim_{r \rightarrow 0} (\sigma_\omega)_{\omega=0} = \lambda r^{\lambda-1} a_r [(1+\lambda) + \chi(1-\lambda)] \quad (6)$$

Substituting the expression into Equation (5),

$$K_I^V = \sqrt{2\pi} a_r \cdot \lambda [(1+\lambda) + \chi(1-\lambda)] \quad (7)$$

Substituting the expression of λ and χ with θ into Equation (7), the relationship between θ and K_I^V can be obtained, as shown in Figure 2a with solid lines. The theoretical calculations agree well with the experimental results, suggesting our proposed method is controllable and reliable to fabricate silicon nanogap array. Using the optimized geometrical parameters, a 90×90

silicon nanogap array (over 1 cm × 1 cm) is achieved, and a typical optical microscopy image is shown in Figure 2b.

Because the notch-concentrated stress induces the local cracking of the notch pairs, that is, forming silicon nanogaps, SERS can be obtained after the functionalization of the silicon nanogap array (over 1 cm × 1 cm) via depositing an ultra-thin Au layer. As shown in Figure 2c, Raman spectra of 10⁻⁴ M RhB are collected from a random point of Au/Si nanogap array, Au/Si ribbon, and Au/PDMS substrate, respectively. As a result, Au/Si nanogap enables significant enhanced Raman signals compared to other scanning samples. The Raman enhancement, RE, is defined as $(I_{\text{SERS}} - I_{\text{bulk}})/I_{\text{bulk}} \times 100\%$, where I_{SERS} and I_{bulk} represent the intensity of Raman scattering peaks obtained from Au/Si nanogap array and Au/Si ribbon, respectively. As a result, RE is calculated to be 2060%, 2060%, 1820% at the Raman shift of 1649.3 cm⁻¹, 1509.2 cm⁻¹, 1362.0 cm⁻¹, respectively. Moreover, this enhancement is strongly depended on the width of silicon nanogap, as shown in Figure 2d. Notably, an obvious RE still appears when the width of nanogap is about 2000 nm, suggesting a promising potential of our fabricated flexible SERS substrate as the platform for sensing large molecules. Detailed Raman spectra of RhB obtained from Au/Si nanogap with different widths can be found in Figure S3, Supporting Information.

The ability of localizing and enhancing the EM field within Au/Si nanogap is crucial for SERS application. As a result, the surface electromagnetic field distribution of Au/Si nanogap under an incident light (514 nm in wavelength) is simulated via finite element analysis (FEA). As shown in Figure 2e, a localized and strong electromagnetic field is observed within the nanogap area, thus allowing for the application in SERS.

Previous report demonstrated that the electromagnetic enhancement within nanogaps is the main contributor to the Raman signal enhancement, and can be expressed as,^[48]

$$E_{\text{EM}} = |E(\omega)|^2 |E(\omega')|^2 \quad (8)$$

where ω and ω' are the incident and scattered frequency, respectively, and $|E(\omega)|$ and $|E(\omega')|$ represent the ratio of local electric field to the incident electromagnetic field at the two frequencies. For qualitative investigations, it is assumed that $\omega \approx \omega'$ as the enhancement at both frequencies are approximately the same. As a result, Equation (8) can be simplified as,

$$E_{\text{EM}} \approx |E|^4 \quad (9)$$

where $|E|$ is the simplification of both $|E(\omega)|$ and $|E(\omega')|$ mentioned in Equation (8).

Therefore, the simulated $|E|^4$ varying with the width of nanogap is investigated. As shown in Figure 2f, $|E|^4$ increases with the decrease of the width of nanogaps, agreeing well with the experimental results shown in Figure 2d. These presented experimental and theoretical results of the relationship between the enhancement in Raman scattering of RhB and the width of nanogaps provide a theoretical basis for further studies about dynamically tunable SERS substrate through controlling the width of nanogaps.

To demonstrate the controllability and reliability of our proposed approach to fabricate silicon nanogap-based SERS

substrates, homogeneities in width and SERS properties of silicon nanogap array over a large area are investigated. In this regard, two strategies involving with and without a vertical loading stress are utilized, as schematically shown in Figure 3a. External vertical loading stress is applied to one edge of the PDMS slab. When peeling off the PDMS stamp without any loading stress, a uniform silicon nanogap array with almost the same width along the ribbon direction is obtained, as shown in Figure 3b with purple dots. However, when a loading stress is applied to the edge of PDMS slab, which just attaches to the released silicon ribbons, an uneven silicon nanogap array with regular variations in width is obtained after the peeling off process. The width of silicon nanogap close to the stress-applied edge becomes much wider, compared to the nanogaps far away from the stress-applied edge (also named as the stress-free edge), as shown in Figure 3b with red dots. The title of x -axis in Figure 3b, that is, relative position, represents the distance between the targeted nanogap and the stress-applied edge.

The applied vertical loading stress can significantly affect the strain distribution of the PDMS slab during the peeling-off process. For the stress-free edge, there is no obvious difference between the situation with or without the loading stress. Therefore, the width of nanogaps at the stress-free edge, W_{SFE} , is almost equal to that of silicon nanogap fabricated without the loading stress, as shown in Figure 3b, implying the effect of loading stress on the stress-free edge is negligible. For the stress-applied edge of PDMS slab, however, the peeling-off stress competes against the vertical loading stress due to the opposite directions. Extra stretching stress exists at the stress-applied edge of PDMS slab, compared to that of PDMS slab without the loading stress. As a result, the width of nanogaps at the stress-applied edge (W_{SAE}) is much larger, that is, $W_{\text{SAE}} > W_{\text{SFE}}$, as shown in Figure 3b. Noting that this extra stretching stress decreases gradually (from the maximum to zero) along the direction from the stress-applied edge to the stress-free edge of PDMS slab, thus, the width of silicon nanogap that is peeled off by the middle region of PDMS slab, named as W_{M} , is larger than W_{SFE} and smaller than W_{SAE} , as shown in Figure 3b. Detailed results about the width of uniform and uneven silicon nanogap arrays at different relative positions are shown in Figures S4–S6, Supporting Information. Figure S4, Supporting Information, shows the optical microscopy images of silicon nanogaps on the uneven nanogap array near (Figure S4a,b, Supporting Information) and far (Figure S4c,d, Supporting Information) from the stress-applied edge. The statistical distributions of nanogap width on uniform and uneven arrays appears in Figure S5a,b, Supporting Information, respectively, and their corresponding SEM images are shown in Figure S6, Supporting Information.

The obtained uniform and uneven silicon nanogap arrays are further explored as SERS substrate through Au layer deposition. Homogenous RE appears at the uniform silicon nanogap array, with an average RE of about 1700%, as displayed in Figure 3c. For the uneven silicon nanogap arrays, the obtained average RE increases from 110% to 1656% with the increase of relative position along x -axis, as shown in Figure 3d. Notably, for both silicon nanogap arrays, RE remains almost unchanged at the same relative position along x -axis, as these nanogaps share the same distance to the stress-applied edge. The divided areas and

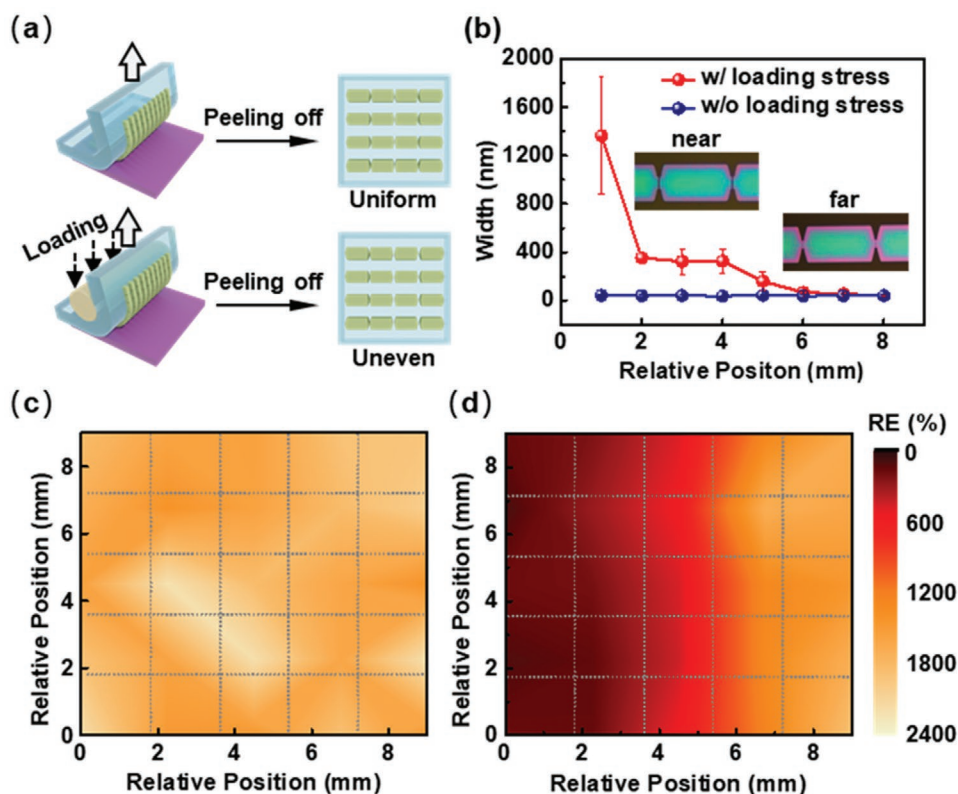


Figure 3. a) Schematic routes for the fabrication of uniform and uneven silicon nanogap arrays. b) The width of silicon nanogap varying with the relative position on the uniform (w/o loading stress, blue dots) and uneven (w/ loading stress, red dots) arrays. Relative position represents the distance between the targeted nanogap and the stress-applied edge. Raman mapping results of RE at 1650 cm^{-1} measured from RhB on: c) a uniform silicon nanogap array-based SERS substrate, and d) an uneven silicon nanogap array-based SERS substrate.

Raman spectra of nanogaps measured in each area are shown in Figure S7, Supporting Information (uniform array) and Figure S8, Supporting Information (uneven array). These presented results may provide guidelines to acquire appropriate SERS substrates for the sense of specific molecules, according to the match of nanogap width and molecular diameter.

It is known that the SERS signals are mainly contributed by the molecules close to the nanogap.^[52,53] The relative location of the measured molecules to the nanogap can influence RE significantly since a nanometer-scale variation in the relative location will cause orders of magnitude change in RE.^[54] In terms of practical applications, common dye molecule, such as Rhodamine, has a relatively small size (several nanometers or smaller). Therefore, extremely narrow nanogaps as the hot spots for SERS are favored to acquire high Raman scattering as well as the high sensitivity. However, for biomacromolecules with the diameter normally ranging from tens to hundreds of nanometers (such as protein molecules), they can hardly access into or even near the hot spots if the width of nanogaps is smaller than the diameter of molecules. As a result, it is difficult to obtain the desired enhancement of Raman scattering. Moreover, even the width of nanogaps is slightly larger than the size of the molecules, the steric hindrance may also prevent the entrance of molecules into the nanogaps.^[55] Therefore, an SERS substrate with controllable and tunable nanogap width in a wide range is necessary for the identification of specific molecules, especially for biomacromolecules.

Because the silicon nanogap array in our work is transferred and directly formed on the PDMS substrate, which is mechanically elastic and flexible, dynamically tunable SERS substrate with tunable nanogap width and RE is in prospect. Demonstration example is realized by in situ Raman measurement of the SERS substrate at thermal heating or cooling conditions, and the thermally induced change in nanogap width is schematically illustrated in Figure 4a. Due to the relatively large thermal expansion coefficient of PDMS, stretch or contraction can be conveniently applied to PDMS through tuning the temperature, thus inducing a widened or shortened width of nanogaps. As shown in Figure 4b, upon the heating treatment, the width of nanogaps broadens due to the expansion of the PDMS, thus enabling the entrance of molecules into the nanogap. After that, the cooling treatment will induce the shrink of the PDMS substrate, thus resulting in a shortened width of nanogaps, and an enhanced Raman scattering signal can be obtained.^[56] Changes of Raman shift intensity with the temperature, which varies from 50 to $-100\text{ }^{\circ}\text{C}$ with a step of $5\text{ }^{\circ}\text{C}$, are shown in Figure 4c. It is found that the Raman shift intensity of our proposed flexible SERS substrate tends to increase with the decrease of the temperature. Slight increase in the intensity of Raman scattering is observed from the counterpart of Au/Si ribbon due to the temperature effect on Raman scattering of RhB,^[57] as shown in Figure S10, Supporting Information. Detailed Raman spectra measured at different temperatures

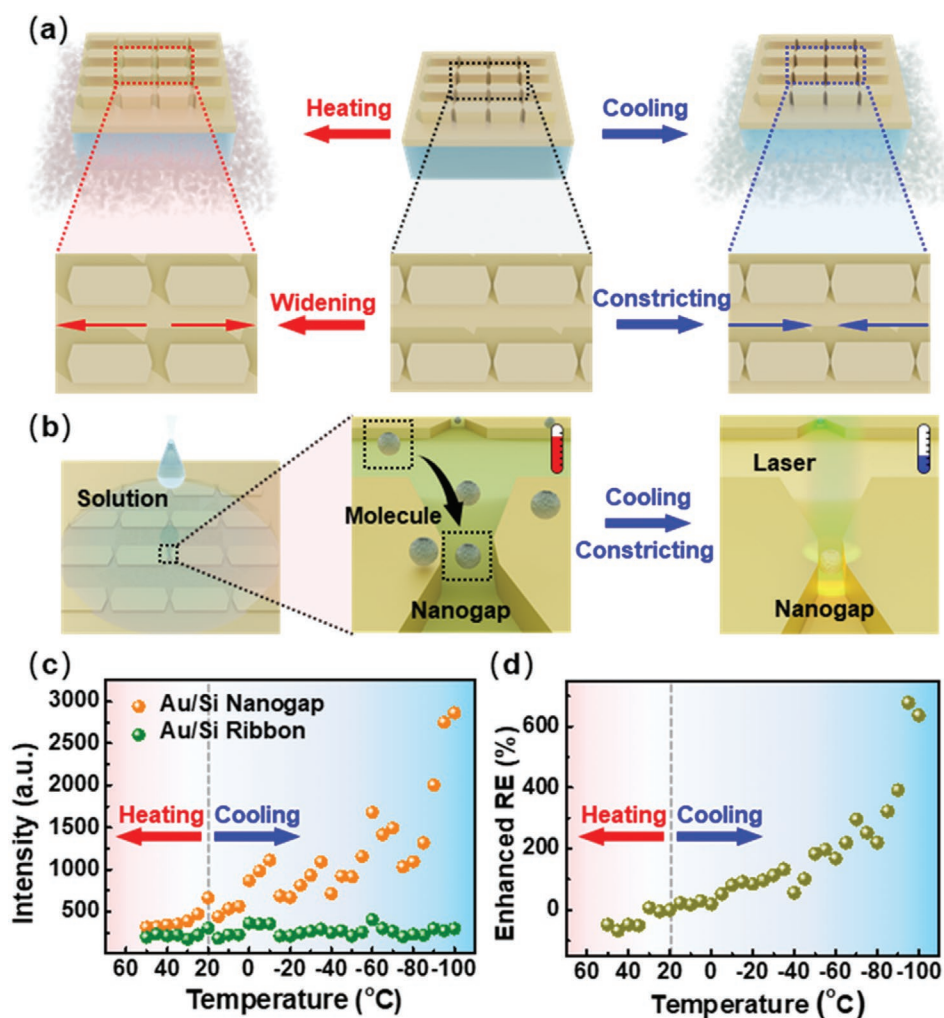


Figure 4. a) Schematic illustration of dynamically tuning the SERS substrate, and the widening and constricting effect can be applied to nanogaps during the heating and cooling process, respectively, thus enabling the tune of SERS properties. b) Schematic illustration of the capture of macromolecules by nanogap with a widened width (high temperature), and the SERS measurement at a shortened width nanogap (low temperature). c) Intensities of the Raman shift (1650 cm^{-1}) measured from Au/Si nanogap and Au/Si ribbon varying with the temperature. d) Enhanced RE of Au/Si nanogap varying with the temperature.

are shown in Figure S11, Supporting Information. Taking the RE calculated from the SERS substrate at $20\text{ }^{\circ}\text{C}$ as the reference, that is, RE_0 , the enhanced RE at a certain temperature is defined as $(RE_T - RE_0)/RE_0 \times 100\%$, where RE_T denotes the Raman enhancement at $T\text{ }^{\circ}\text{C}$. Figure 4d shows the enhanced RE varying with the temperature. In particular, the enhanced RE reaches 636% at $-100\text{ }^{\circ}\text{C}$. The demonstrated dynamically tunable SERS substrate exhibits great potentials for improving the sensitivity during an in-situ measurement, as well as the identification of molecules with different sizes.

3. Conclusion

In summary, we developed a simple and convenient approach to fabricate a silicon nanogap-based dynamically tunable SERS substrate for molecular sensing. Scalable production of silicon nanogaps with controllable width, and the ability of dynamically

tuning the SERS properties for molecular sensing in platforms that are realized by a loading-stress approach or the thermal treatment, represent the main points of interest. Systemic experimental and theoretical studies reveal the key geometrical design considerations to realize a silicon nanogap array with high yield and controllable width. Both experiments and simulations demonstrate that the Raman enhancement of flexible SERS substrate, constructed with the functionalized silicon nanogap array, is strongly determined by the width of silicon nanogap. The ability of constructing a single SERS substrate with different widths of nanogaps enables the sense of various molecules with a wide size range. Dynamically tunable SERS substrate could improve the sensitivity during an in situ measurement. These results provide an attractive solution for the challenge of dynamically tunable SERS substrate for molecular sensing, thereby accelerating the development of different classes of SERS substrates, with great potentials for environmental monitoring and biochemical detection.

4. Experimental Section

Preparation of Silicon Nanogap-Based SERS Substrate: (100) SOI wafers (Top silicon: 100 nm and buried oxide: 145 nm) were used to fabricate silicon nanogap-based dynamically tunable SERS substrates. After the ultrasonic cleaning with acetone, ethanol, and deionized water, the SOI wafer was defined with an array of notch pairs within silicon ribbon (50 μm in width) by photolithography and reactive ion etching (RIE), and the spacing between two neighboring periodical notch pairs was 100 μm . In this process, photoresist (AZ-5214) was spin-coated at 3000 rpm for 30 s, and O_2/SF_6 (3/15 sccm) was used as etching gases for 120 s at a pressure of 100 mTorr. After the removal of buried oxide by immersing the patterned SOI in HF solution (30%), silicon ribbons with periodic notch pairs were released on the substrate. Then, PDMS (Sylgard-184, Dow Corning, thickness ≈ 1 mm) slabs were prepared by mixing base A and curing agent B in a ratio of 10:1, which were fully cured at 80 $^\circ\text{C}$ for 2 h. After forming a conformal contact with the patterned SOI, peeling-off the PDMS slab at a speed of about 10 cm s^{-1} led to the transfer of silicon ribbons with notch pairs, and silicon nanogaps formed simultaneously. Then, a 30 nm thick Au layer was deposited by electron beam evaporation at a rate of 0.1 \AA s^{-1} , and the flexible silicon nanogap-based SERS substrate was fabricated and put aside for the following application in molecular sensing.

Optimization of the Geometrical Design of Notch Pairs: Because the yield of silicon nanogaps during the transfer process was strongly depended on the geometry of notch pairs, key parameters including the notch angle (defined as the angle between two sides of a notch) and tip distance of a notch pair were optimized. The width of silicon ribbons was defined as 50 μm . A set of notch angles, including 30 $^\circ$, 45 $^\circ$, 60 $^\circ$, 75 $^\circ$, 90 $^\circ$, and 120 $^\circ$, and a set of tip distances, including 5 μm , 10 μm , and 15 μm , were investigated to optimize the geometrical design of notch pairs. The yield of nanogap of different distances and notch angles was obtained by counting the number of cracks existing in the notch pairs of the as-prepared 20 \times 20 notch pair arrays after the peeling off.

Characterizations: Morphologies of silicon nanogap arrays were characterized using an optical microscope (OLYMPUS BX51) and a scanning electron microscope (SEM, Zeiss Sigma). For the SERS characterization, flexible silicon nanogap-based molecular sensing array was dipped in 10^{-4} M RhB aqueous for 2 min, then the solvent was prudently wiped up. Raman spectrum was obtained by Raman scattering spectrometer (HORIBA LabRAM HR800), and the wavelength of the excitation laser was 514.65 nm, with a focused spot diameter of about 1 μm . For dynamically tuning the SERS substrate via a thermal treatment, the temperature was controlled by a heating and freezing microscope stage (Linkam THMS600) linked with a temperature controller (Linkam T95-PE). A liquid nitrogen container was linked with the stage too. The flexible SERS substrate could be heated by the metal heater in the stage, and cooled as the liquid nitrogen evaporated. The cooling/heating rate was precisely controlled by a temperature controller. Then, Raman spectra of the flexible SERS substrate were collected in situ under different temperatures. Au/Si ribbons were also measured at the same condition for comparison.

Electromagnetic Simulation: The finite element analysis was used to study the surface electromagnetic field distribution of Au/Si nanogap. The simulation was performed using the commercial software COMSOL Multiphysics. The type of mesh was free tetrahedral in active domains and free triangular in boundaries. The incident plane wave was defined by a periodic port, and the side boundaries were periodical with Floquet condition from a periodic port. The electromagnetic parameters of Au and Si were available in the material library of COMSOL, which were directly used in the simulation. The electromagnetic parameters of PDMS were referred to in previous literature.^[58] All the parameters in the modeling, such as the thicknesses of Au and silicon, the width of nanogaps, and other related, were used as the same as in the experiment.

Supporting Information

Supporting Information is available from the Wiley Online Library or from the author.

Acknowledgements

This work was supported by the Natural Science Foundation of China (Nos. 51961145108, 61975035, and 51850410502), the Science and Technology Commission of Shanghai Municipality (Nos. 19XD1400600, 20501130700, and 19JC1415500), the Qilu Young Scholar Program of Shandong University, the State Key Laboratory of ASIC & System (Grant No. 2020KF007), the State Key Laboratory of Functional Materials for Informatics (Grant No. SKL202101), and the Shandong University Multidisciplinary Research and Innovation Team of Young Scholars (No. 2020QNQT015).

Conflict of Interest

The authors declare no conflict of interest.

Data Availability Statement

The data that support the findings of this study are available from the corresponding author upon reasonable request.

Keywords

dynamically tunable SERS, flexible electronics, molecule sensing, scalable silicon nanogap array, transfer printing

Received: April 22, 2021

Revised: June 15, 2021

Published online: July 20, 2021

- [1] P. Gu, W. Zhang, G. Zhang, *Adv. Mater. Interfaces* **2018**, *5*, 1800648.
- [2] B. Ai, Y. Yu, H. Moehwald, G. Zhang, B. Yang, *Adv. Colloid Interface Sci.* **2014**, *206*, 5.
- [3] H. Cai, Y. Wu, Y. Dai, N. Pan, Y. Tian, Y. Luo, X. Wang, *Opt. Express* **2016**, *24*, 20808.
- [4] N. Liu, M. L. Tang, M. Hentschel, H. Giessen, A. P. Alivisatos, *Nat. Mater.* **2011**, *10*, 631.
- [5] S. Kim, J. Jin, Y.-J. Kim, I.-Y. Park, Y. Kim, S.-W. Kim, *Nature* **2008**, *453*, 757.
- [6] J.-H. Lee, J.-W. Oh, S. H. Nam, Y. S. Cha, G.-H. Kim, W.-K. Rhim, N. H. Kim, J. Kim, S. W. Han, Y. D. Suh, J.-M. Nam, *Small* **2016**, *12*, 4726.
- [7] J. W. Kang, P. T. C. So, R. R. Dasari, D.-K. Lim, *Nano Lett.* **2015**, *15*, 1766.
- [8] W. Cai, J. S. White, M. L. Brongersma, *Nano Lett.* **2009**, *9*, 4403.
- [9] V. Dubois, S. J. Bleiker, G. Stemme, F. Niklaus, *Adv. Mater.* **2018**, *30*, 1801124.
- [10] S. V. Aradhya, L. Venkataraman, *Nat. Nanotechnol.* **2013**, *8*, 399.
- [11] C. Joachim, J. K. Gimzewski, A. Aviram, *Nature* **2000**, *408*, 541.
- [12] E. C. Le Ru, P. G. Etchegoin, *Annu. Rev. Phys. Chem.* **2012**, *63*, 65.
- [13] Z. Zuo, S. Zhang, Y. Wang, Y. Guo, L. Sun, K. Li, G. Cui, *Nanoscale* **2019**, *11*, 17913.
- [14] F. Qin, T. Zhao, R. B. Jiang, N. N. Jiang, Q. F. Ruan, J. F. Wang, L. D. Sun, C. H. Yan, H. Q. Lin, *Adv. Opt. Mater.* **2016**, *4*, 76.

- [15] L. S. Slaughter, B. A. Willingham, W.-S. Chang, M. H. Chester, N. Ogden, S. Link, *Nano Lett.* **2012**, *12*, 3967.
- [16] J.-H. Tian, B. Liu, X. Li, Z.-L. Yang, B. Ren, S.-T. Wu, N. Tao, Z.-Q. Tian, *J. Am. Chem. Soc.* **2006**, *128*, 14748.
- [17] H. Le-The, J. J. A. Lozeman, M. Lafuente, P. Munoz, J. G. Bomer, D.-T. Hien, E. Berenschot, A. van den Berg, N. R. Tas, M. Odijk, J. C. T. Eijkel, *Nanoscale* **2019**, *11*, 12152.
- [18] T. A. Green, *Gold Bull.* **2014**, *47*, 205.
- [19] W. Zhu, K. B. Crozier, *Nat. Commun.* **2014**, *5*, 5228.
- [20] M. Melli, A. Polyakov, D. Gargas, C. Huynh, L. Scipioni, W. Bao, D. F. Ogletree, P. J. Schuck, S. Cabrini, A. Weber-Bargioni, *Nano Lett.* **2013**, *13*, 2687.
- [21] J. M. Hoffmann, H. Janssen, D. N. Chigrin, T. Taubner, *Opt. Express* **2014**, *22*, 14425.
- [22] S. Kubatkin, A. Danilov, M. Hjort, J. Cornil, J. L. Bredas, N. Stuhr-Hansen, P. Hedegard, T. Bjornholm, *Nature* **2003**, *425*, 698.
- [23] M. Im, J.-H. Ahn, J.-W. Han, T. J. Park, S. Y. Lee, Y.-K. Choi, *IEEE Sens. J.* **2011**, *11*, 351.
- [24] X. Chen, H.-R. Park, M. Pelton, X. Piao, N. C. Lindquist, H. Im, Y. J. Kim, J. S. Ahn, K. J. Ahn, N. Park, D.-S. Kim, S.-H. Oh, *Nat. Commun.* **2013**, *4*, 2361.
- [25] A. Cui, Z. Liu, H. Dong, F. Yang, Y. Zhen, W. Li, J. Li, C. Gu, X. Zhang, R. Li, W. Hu, *Adv. Mater.* **2016**, *28*, 8227.
- [26] V. Dubois, S. N. Raja, P. Gehring, S. Caneva, H. S. J. van der Zant, F. Niklaus, G. Stemme, *Nat. Commun.* **2018**, *9*, 3433.
- [27] V. Dubois, F. Niklaus, G. Stemme, *Microsyst. Nanoeng.* **2017**, *3*, 17042.
- [28] I. Fernandez-Martinez, Y. Gonzalez, F. Briones, *Nanotechnology* **2008**, *19*, 275302.
- [29] R. Pan, Y. Yang, Y. Wang, S. Li, Z. Liu, Y. Su, B. Quan, Y. Li, C. Gu, J. Li, *Nanoscale* **2018**, *10*, 3171.
- [30] K. Xu, R. Zhou, K. Takei, M. Hong, *Adv. Sci.* **2019**, *6*, 1900925.
- [31] M. G. Albrecht, J. A. Creighton, *J. Am. Chem. Soc.* **1977**, *99*, 5215.
- [32] M. Fleischmann, P. J. Hendra, A. J. McQuillan, *Chem. Phys. Lett.* **1974**, *26*, 163.
- [33] S. Kumar, D. K. Lodhi, P. Goel, P. M. Neeti, J. P. Singh, *Chem. Commun.* **2015**, *51*, 12411.
- [34] H. Kang, C.-J. Heo, H. C. Jeon, S. Y. Lee, S.-M. Yang, *ACS Appl. Mater. Interfaces* **2013**, *5*, 4569.
- [35] S. Li, M. L. Pedano, S.-H. Chang, C. A. Mirkin, G. C. Schatz, *Nano Lett.* **2010**, *10*, 1722.
- [36] A. Cui, Z. Liu, H. Dong, Y. Wang, Y. Zhen, W. Li, J. Li, C. Gu, W. Hu, *Adv. Mater.* **2015**, *27*, 3002.
- [37] J. W. Jeong, S. R. Yang, Y. H. Hur, S. W. Kim, K. M. Baek, S. Yim, H.-I. Jang, J. H. Park, S. Y. Lee, C.-O. Park, Y. S. Jung, *Nat. Commun.* **2014**, *5*, 5387.
- [38] S. Si, W. Liang, Y. Sun, J. Huang, W. Ma, Z. Liang, Q. Bao, L. Jiang, *Adv. Funct. Mater.* **2016**, *26*, 8137.
- [39] Z. Li, G. Meng, Q. Huang, X. Hu, X. He, H. Tang, Z. Wang, F. Li, *Small* **2015**, *11*, 5452.
- [40] M. Kahraman, P. Daggumati, O. Kurtulus, E. Seker, S. Wachsmann-Hogiu, *Sci. Rep.* **2013**, *3*, 3396.
- [41] Y. Chen, Q. Guo, G. Huang, G. Li, L. Wang, Z. Tian, Y. Qin, Z. Di, Y. Mei, *ACS Appl. Mater. Interfaces* **2018**, *10*, 25644.
- [42] Q. Guo, M. Zhang, Z. Xue, G. Wang, D. Chen, R. Cao, G. Huang, Y. Mei, Z. Di, X. Wang, *Small* **2015**, *11*, 4140.
- [43] Q. Guo, M. Zhang, Z. Xue, L. Ye, G. Wang, G. Huang, Y. Mei, X. Wang, Z. Di, *Appl. Phys. Lett.* **2013**, *103*, 264102.
- [44] F. J. Gomez, M. Elices, *Int. J. Fract.* **2003**, *123*, 163.
- [45] B. Atzori, P. Lazzarin, S. Filippi, *Int. J. Fatigue* **2001**, *23*, 355.
- [46] F. Qin, T. Zhao, R. Jiang, N. Jiang, Q. Ruan, J. Wang, L. Sun, C.-H. Yan, H.-Q. Lin, *Adv. Opt. Mater.* **2016**, *4*, 76.
- [47] D. Choi, Y. Choi, S. Hong, T. Kang, L. P. Lee, *Small* **2010**, *6*, 1741.
- [48] J. M. McMahon, S. Li, L. K. Ausman, G. C. Schatz, *J. Phys. Chem. C* **2012**, *116*, 1627.
- [49] E. Tanne, T. Li, B. Bourdin, J. J. Marigo, C. Maurini, *J. Mech. Phys. Solids* **2018**, *110*, 80.
- [50] P. Lazzarin, R. Tovo, *Int. J. Fract.* **1996**, *78*, 3.
- [51] B. Gross, A. Mendelson, *Int. J. Fract. Mech.* **1972**, *8*, 267.
- [52] H. Lu, L. Zhu, C. Zhang, K. Chen, Y. Cui, *Anal. Chem.* **2018**, *90*, 4535.
- [53] M. S. Schmidt, J. Hubner, A. Boisen, *Adv. Mater.* **2012**, *24*, OP11.
- [54] A. B. Zrimsek, N. Chiang, M. Mattei, S. Zaleski, M. O. McAnally, C. T. Chapman, A.-I. Henry, G. C. Schatz, R. P. van Duyne, *Chem. Rev.* **2017**, *117*, 7583.
- [55] H. Liu, Z. Yang, L. Meng, Y. Sun, J. Wang, L. Yang, J. Liu, Z. Tian, *J. Am. Chem. Soc.* **2014**, *136*, 5332.
- [56] H. Mitomo, K. Horie, Y. Matsuo, K. Niikura, T. Tani, M. Naya, K. Ijiri, *Adv. Opt. Mater.* **2016**, *4*, 259.
- [57] L. Zhou, J. Zhou, W. Lai, X. Yang, J. Meng, L. Su, C. Gu, T. Jiang, E. Y. B. Pun, L. Shao, L. Petti, X. W. Sun, Z. Jia, Q. Li, J. Han, P. Mormile, *Nat. Commun.* **2020**, *11*, 1785.
- [58] S. U. Zhang, *Microelectron. Reliab.* **2015**, *55*, 2678.